GEOPHYSICAL RESEARCH LETTERS, VOL. 37, L13101, doi:10.1029/2010GL044140, 2010

Energetic neutral atoms from the Earth's subsolar magnetopause

S. A. Fuselier,[1] H. O. Funsten,[2] D. Heirtzler,[3] P. Janzen,[4] H. Kucharek,[3] D. J. McComas,[5,6] E. Möbius,[3] T. E. Moore,[7] S. M. Petrinec,[1] D. B. Reisenfeld,[4] N. A. Schwadron,[8] K. J. Trattner,[1] and P. Wurz[9]

Received 28 May 2010; accepted 8 June 2010; published 8 July 2010.

[1] The shocked solar wind in the Earth's magnetosheath becomes nearly stationary at the subsolar magnetopause. At this location, solar wind protons are neutralized by charge exchange with neutral hydrogen atoms at the extreme limits of the Earth's tenuous exosphere. The resulting Energetic Neutral Atoms (ENAs) propagate away from the subsolar region in nearly all directions. Simultaneous observations of hydrogen ENAs from the Interstellar Boundary Explorer (IBEX) and proton distributions in the magnetosheath from the Cluster spacecraft are used to quantify this charge exchange process. By combining these observations with a relatively simple model, estimates are obtained for the ratio of ENA to shocked solar wind flux (about 10^{-4}) and the exospheric density at distances greater than 10 Earth Radii (R_E) upstream from the Earth (about 8 cm^{-3}). **Citation:** Fuselier, S. A., et al. (2010), Energetic neutral atoms from the Earth's subsolar magnetopause, *Geophys. Res. Lett.*, *37*, L13101, doi:10.1029/2010GL044140.

1. Introduction

[2] The shocked solar wind is diverted around the magnetosphere in the Earth's magnetosheath. Diversion begins at the bow shock, where the solar wind is heated, slowed, and deflected. The distance of the bow shock from the Earth depends on solar wind dynamic pressure, but is typically 14–15 R_E at the subsolar point (i.e., along the aberrated Earth-Sun line). Further slowing of the shocked solar wind occurs in the magnetosheath so that when the subsolar magnetopause is reached (at an average distance of ~10 R_E [e.g., *Shue et al.*, 1998]), the shocked solar wind density is very high, the plasma is nearly stationary, and most of the ~1 keV bulk flow energy goes into plasma heating. Throughout this region, the conductivity is very high, so the interplanetary magnetic field (IMF) is "frozen in" the plasma, and both field and plasma must ultimately divert together around the magnetopause.

[3] Characteristics of subsolar magnetosheath proton distributions depend on the angle θ_{Bn} between the shock normal and the IMF at the subsolar point. When $\theta_{Bn} > 45°$, up to 20% of solar wind protons specularly reflect off the shock front, gyrate into the upstream region, and return to the shock with considerably higher energy. These protons are transmitted into the magnetosheath along with the heated core of the solar wind to produce a two-component proton distribution [*Gosling and Robson*, 1985]. This two-component proton distribution can survive up to the magnetopause [e.g., *Fuselier et al.*, 1988]. When $\theta_{Bn} < 45°$, a similar two-component lower-energy proton distribution is produced and there is an additional, third component at higher energies (>10 keV) from shock acceleration [*Gosling et al.*, 1989].

[4] At the subsolar magnetopause, the lower-energy two-component proton population is nearly stationary. Unless it crosses the magnetopause, the shocked solar wind plasma is the closest to the Earth for any nearly stationary proton population with significant input flux. At this location, the proton population has the highest probability of interacting with the Earth's exospheric cold, neutral hydrogen population (whose density decreases approximately as $1/R^3$ from the Earth). Shocked solar wind protons charge exchange with exospheric hydrogen atoms, producing ENAs. These ENAs are not bound to the magnetosheath magnetic field and follow ballistic trajectories with direction and speed equal to their velocity at the time of charge exchange. Therefore, they retain information about source proton populations.

[5] The Low Energy Neutral Atom (LENA) imager [*Moore et al.*, 2000] on the Imager for Magnetopause to Aurora: Global Exploration (IMAGE) spacecraft was likely first to detect ENAs from the Earth's subsolar magnetopause. The LENA imager did not have sufficient energy resolution nor were there any simultaneous magnetosheath observations to quantify the process. However, observations showed that ENAs emanating from the subsolar direction were correlated with solar wind dynamic pressure [*Collier et al.*, 2005; *Taguchi et al.*, 2005; *Hosokawa et al.*, 2008]. This correlation, together with the arrival direction of ENAs strongly suggested that ENAs were from the shocked solar wind.

[6] In this paper, simultaneous observations of energy-resolved hydrogen ENA distributions from the subsolar magnetosheath direction and proton distributions in the Earth's magnetosheath are used to analyze and quantify the shocked solar wind charge exchange process. These observations and a relatively simple model are used to estimate the ion to ENA flux ratio and the exospheric

[1]Lockheed Martin Advanced Technology Center, Palo Alto, California, USA.
[2]Los Alamos National Laboratory, Los Alamos, New Mexico, USA.
[3]Institute for the Study of Earth, Oceans and Space, University of New Hampshire, Durham, New Hampshire, USA.
[4]Department of Physics and Astronomy, University of Montana, Billings, Montana, USA.
[5]Southwest Research Institute, San Antonio, Texas, USA.
[6]University of Texas, San Antonio, Texas, USA.
[7]Heliophysics Science Division, NASA Goddard Space Flight Center, Greenbelt, Maryland, USA.
[8]Astronomy Department, Boston University, Boston, Massachusetts, USA.
[9]Physics Institute, University of Bern, Bern, Switzerland.

0094-8276/10/2010GL044140

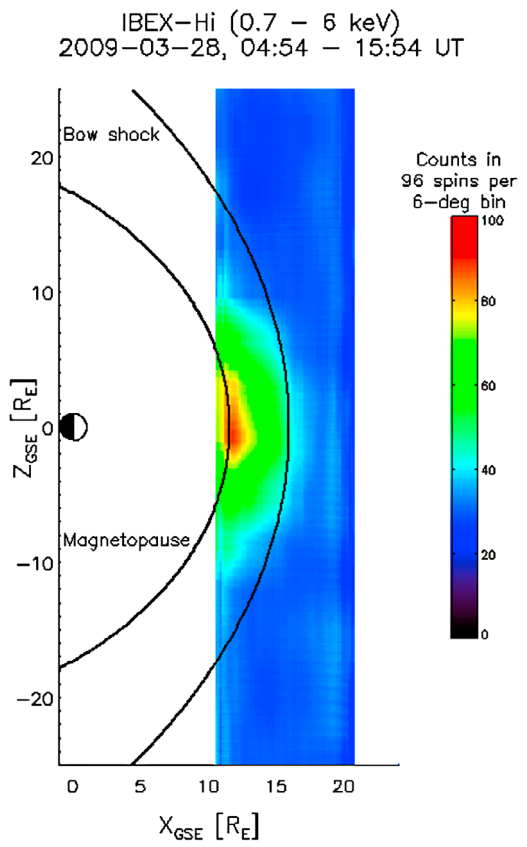

Figure 1. Hydrogen ENA countrate integrated from 0.7–6 keV on 28 March 2009 from 04:54–15:54 UT. The peak is centered on the subsolar magnetopause. Significant flux extends to nearly ±10 R_E in the Z_{GSE} direction.

hydrogen density at a distance of ~10 R_E upstream from the Earth.

2. Simultaneous ENA and Proton Observations

[7] ENA observations are from the Interstellar Boundary Explorer (IBEX) mission [*McComas et al.*, 2009a]. IBEX is primarily focused on the global interaction between the solar wind and the interplanetary medium (see *McComas et al.* [2009b] and associated papers). However, the small explorer also obtains extremely high sensitivity and energy resolved observations of other, "local" ENA sources including the Moon [*McComas et al.*, 2009c], the terrestrial magnetosphere, and, in this study, the magnetosheath. IBEX has two high-sensitivity, single-pixel ENA cameras covering energies from 0.01 to 6 keV, with significant energy overlap around 1 keV [*Funsten et al.*, 2009; *Fuselier et al.*, 2009]. The spacecraft is in a highly elliptical, nearly equatorial orbit with apogee of almost 50 R_E and perigee of 2–4 R_E (geocentric). The spacecraft spin axis points within a few degrees of the Sun and the cameras' FWHM 7° × 7° fields-of-view (FOV) are perpendicular to the spin axis. As the spacecraft spins, the cameras' FOV scribe a circle in the sky. For two time intervals a year (in November/December and March/April), the ENA cameras have prolonged views of the subsolar magnetopause. Intervals include several of the 7.5-day orbits and, during an orbit, the cameras view the subsolar magnetopause nearly continuously for periods ranging from several hours to days.

[8] Figure 1 shows Hydrogen ENA observations projected into the X-Z_{GSE} plane from one of these prolonged intervals on 28 March 2009. The 11 R_E subsolar magnetopause location in Figure 1 was determined from the *Shue et al.* [1998] magnetopause model with solar wind dynamic pressure of 1.1 nPa (from WIND spacecraft observations, [*Ogilvie et al.*, 1995]) and no IMF. During the 11 h period, the solar wind was very steady. The speed was 390 ± 7 km/s and the density was 4.2 ± 0.5 cm^{-3}. With these stable conditions,

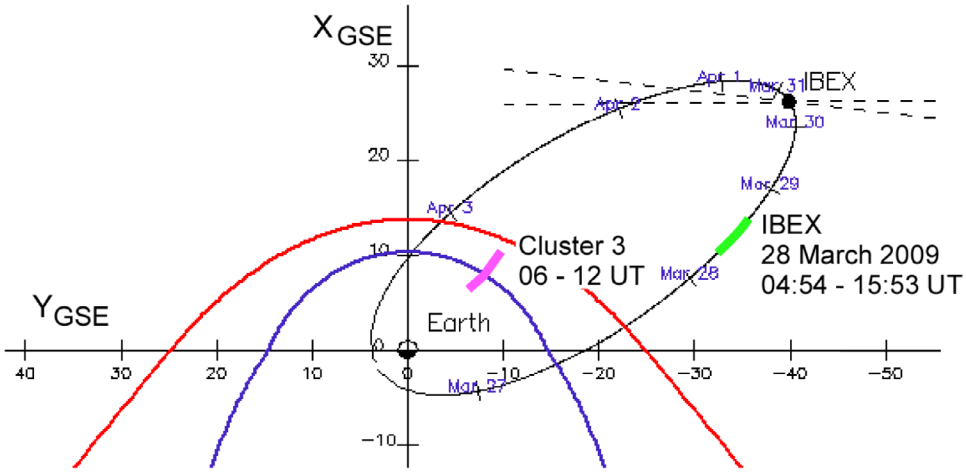

Figure 2. IBEX and Cluster 3 spacecraft orbits projected into the ecliptic plane. The IBEX cameras' FOV included the subsolar magnetopause on 28 March 2009 from 04:54 – 15:53 UT. During the first part of that interval, the Cluster 3 spacecraft was in the magnetosheath measuring the parent proton population for ENAs observed by IBEX (see Figure 1).

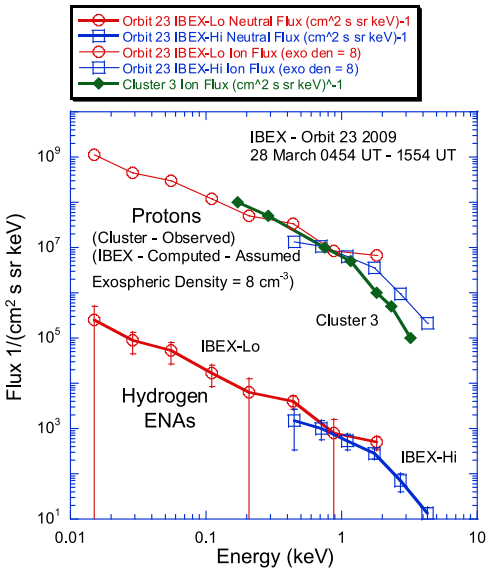

Figure 3. Proton and ENA fluxes observed by Cluster 3 and IBEX on 28 March 2009. Lower curves show ENA fluxes observed by IBEX. The upper green curve (solid diamonds) shows magnetosheath proton fluxes observed by Cluster 3. Two upper curves (red for IBEX-Lo and blue for IBEX-Hi) are proton fluxes computed from ENA fluxes. Computed and observed proton fluxes agree well for an exospheric hydrogen density at 10 R_E geocentric distance of 8 cm^{-3}.

the subsolar magnetopause was steady at 11 ± 0.2 R_E over the time interval.

[9] To create the spatial map of ENA flux, orthogonal angles are used. A single spin is comprised of sixty 6° bins; each 7° wide (representing the camera FOV). Because of slow precession of the IBEX spacecraft attitude vector with respect to the Earth, there is substantial overlap of angular bins from spin to spin. A composite ENA image over 11 h is thus created from many spins and projected into the GSE noon-midnight meridinal plane. The composite image therefore appears to have much greater resolution than the 6° × 7° angular bins of a single spin.

[10] In Figure 1, ENA fluxes peak along the Earth-Sun line at the calculated location of the subsolar magnetopause. Fluxes fall off relatively rapidly in both vertical (Z_{GSE}) and Earth-Sun (X_{GSE}) directions. Figure 2 shows the ecliptic plane projection of the IBEX orbit for the time interval in Figure 1, nominal bow shock and magnetopause locations, and the ecliptic plane FOV of the IBEX cameras. Also shown is the ecliptic plane projection of the Cluster 3 spacecraft as it traversed the magnetosheath during the 11-h period used for Figure 1. Cluster was located ~10 R_E below ($-Z_{GSE}$) the ecliptic plane.

[11] IBEX-Hi and −Lo resolve ENA fluxes into broad energy channels (6 for −Hi and 8 for −Lo) covering 0.01 to 6 keV. The lower two curves in Figure 3 show neutral hydrogen flux versus energy (averaged over the 11-h interval and the three pixels surrounding the subsolar magnetopause) as measured by IBEX-Hi and −Lo cameras (open squares and circles, respectively). Error bars on ENA fluxes are the larger of statistical uncertainties in counts, 50% uncertainty in absolute flux for IBEX-Lo for energies below 0.2 keV, or 30% uncertainty in absolute flux for IBEX-Lo above 0.2 keV and for IBEX-Hi over all energies.

[12] The ENA spectrum has two components. The lower energy component extends from 0.01 to ~1 keV and the higher energy component starts at about 1 keV. The break in the energy spectrum at 1 keV and more rapid decrease above 2 keV are characteristic of proton spectra observed in the magnetosheath [e.g., *Gosling and Robson*, 1985; *Fuselier et al.*, 1988].

[13] In general, ENA and ion fluxes are related by (1),

$$J_{ENA}(E,x,z) = \int J_{ion}(E,x,y,z)\sigma(E)n_H(x,y,z)dy \qquad (1)$$

where $J_{ENA}(E,x,z)$ is the ENA flux, $J_{ion}(E,x,y,z)$ is the ion flux (which depends on both energy and Y_{GSE}), $\sigma(E)$ is the energy-dependent charge-exchange cross-section (here for $H^+ + H^0 \rightarrow H^0 + H^+$), $n_H(x,y,z)$ is the exospheric neutral hydrogen density, (which also depends on Y_{GSE}), and the integral is done over the column length, which is essentially in the Y_{GSE} direction (see Figure 2). From 0.01 to 6 keV, the energy range of the IBEX sensors, the proton on hydrogen cross-section decreases from about 4 × 10^{-15} cm^{-2} to 1 × 10^{-15} cm^{-2} [*Lindsay and Stebbings*, 2005].

[14] Proton fluxes and exospheric neutral hydrogen densities are functions of distance from the subsolar magnetopause and radial distance from the Earth, respectively. Models for these proton fluxes and neutral hydrogen densities are needed to evaluate the integral in (1). Here, (1) is simplified by first assuming that the proton flux (in the plasma rest frame) depends only on energy and not on distance from the subsolar point along the Y_{GSE} direction. This assumption allows direct comparison between ENA fluxes observed by IBEX and proton fluxes observed by Cluster and removes $J_{ion}(E)$ from the integral (1). Second, it is assumed that the exospheric density decreases as $1/R^3$ from the subsolar point [e.g., *Collier et al.*, 2001], so that

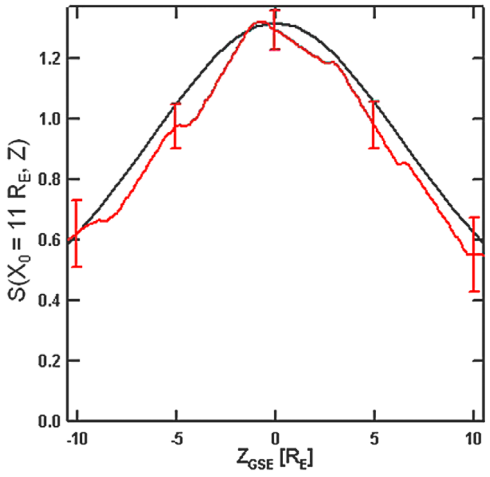

Figure 4. Comparison between ENA countrate profile from Figure 1 (red curve) and S(x = 11 R_E, z) (black curve) from (3). The two profiles compare reasonably well, indicating that the assumptions that were made to derive (3) are valid over distances of the order of 10 R_E.

Table 1. ENA Fluxes and Computed Exospheric Densities for Several Intervals in 2009

IBEX Orbit (Dates)	IBEX ENA flux at 1 keV (cm^{-2} s sr keV)$^{-1}$	Derived Exospheric Neutral Hydrogen Density (atoms/cm^3)
21 (11 March 2009 2310 UT – 12 March 2009 0840 UT)	530	4
23 (28 March 2009 0554 UT – 1554 UT)	600	8
24 (5 April 2009 0110 UT – 2300 UT)	2000	8
25 (13 April 2009 1810 UT – 14 April 2010 0915 UT)	2300	11

$n_H(x,y,z) = n_{H0}\ R_0^3/\ (x^2 + y^2 + z^2)^{3/2}$, where $R_0 = 10\ R_E$ (the subsolar point). With this assumption, the integral in (1) (integrated from $y = -10\ R_E$ to $+10\ R_E$) is solved analytically to yield:

$$J_{ENA}(E, x, z) = J_{ion}(E)\sigma(E)n_{H0}R_0S(x, z) \quad (2)$$

where,

$$S(x, z) = R_0^2/(x^2 + z^2)2(10R_E/\sqrt{(x^2 + z^2 + (10\ R_E)^2}) \quad (3)$$

Since $J_{ENA}(E,x,z)$ and S(x,z) are the only quantities in (2) that depend on position, the ENA flux profile at fixed x is directly comparable to S(x,z). Figure 4 shows this comparison, where the observed ENA flux profile in the z direction in Figure 1 was normalized to S($x = 11\ R_E$, $z = 0$). While ENA fluxes decrease somewhat faster than S(x,z), the two curves are similar from $-10\ R_E$ to $10\ R_E$. This similarity provides justification for assumptions used to derive (2).

[15] Proton fluxes computed from ENA fluxes and (2) and proton fluxes observed by the Cluster 3 spacecraft (obtained by averaging fluxes in the plasma rest frame for 3 intervals spanning the period when Cluster 3 was in the magnetosheath) are compared in Figure 3, for an exospheric density at $10\ R_E$, $n_{H0} = 8\ cm^{-3}$. Computed and observed fluxes compare well over the observed energy range and both spectra show a break at near 1 keV, consistent with the two-component proton spectrum that is typically observed in the Earth's magnetosheath [*Gosling and Robson*, 1985]. Overall, the ratio of hydrogen ENA to proton flux depends on energy; however, from 0.01 to 6 keV, it is nearly constant at about 10^{-4}.

[16] IBEX observed ENAs from the subsolar magnetopause for several intervals over several orbits in spring 2009. For each interval, the solar wind conditions were relatively stable and Cluster observations in the magnetosheath were available to compare ENA and proton fluxes and determine exospheric densities using (2). Table 1 shows these intervals, observed ENA fluxes at 1 keV, and estimates of exospheric neutral hydrogen densities. Exospheric densities at the subsolar magnetopause range from 4 to 11 cm^{-3}, with uncertainties of the order of ±1–2 cm^{-3}, based on uncertainties in ENA fluxes measured by IBEX. Given these uncertainties, exospheric neutral densities are quite consistent from orbit to orbit during a period when there were no significant changes in the solar wind conditions.

3. Conclusions

[17] Comparison of simultaneous ENA and proton spectra in Figure 3 quantifies the subsolar magnetopause charge exchange process. The ENA to proton flux ratio is about 10^{-4}, (1.5×10^{-4} at 1 keV, see Figure 3) which is on the low end of the 10^{-3} to 10^{-4} estimate from IMAGE/LENA observations that assumed average solar wind conditions [*Collier et al.*, 2001], but consistent with ENA to proton flux ratios from the Earth's magnetospheric cusps [*Taguchi et al.*, 2005]. The observed proton spectrum and the proton spectrum computed from IBEX ENA observations and (2) are comparable for exospheric neutral hydrogen densities of 4–11 cm^{-3} at the subsolar magnetopause (i.e., ~$10\ R_E$ geocentric distance along the Earth-Sun line). These exospheric densities were obtained from a relatively simple model. A more sophisticated model is needed to evaluate the complete integral in (1). In particular, the model should include changes in both the exospheric density with radial distance from the Earth and changes in magnetosheath proton density with distance from the subsolar magnetopause. For example, magnetosheath densities decrease by a factor of 0.7 along the magnetopause from the subsolar point to $10\ R_E$ away [*Petrinec and Russell*, 1997]. This decrease will reduce the estimated exospheric density at the subsolar point by approximately the same amount. Proton density is not the only factor that affects observed ENA fluxes. For example, the magnetosheath proton population is typically anisotropic, with $T_\perp/T_\parallel \sim 1.5$ [e.g., *Anderson et al.*, 1994]. This anisotropy will affect ENA fluxes observed from dawn or dusk vantage points of the IBEX spacecraft. For example, if the IMF is northward, then ENA fluxes may be higher because the parent proton distribution is anisotropic. However, improvements like these in the model probably do not amount to more than a factor of 2 increase or decrease in exospheric densities derived from the simple model and shown in Table 1.

[18] Finally, using Lyman Alpha observations, *Østgaard et al.* [2003] and, more recently, *Zoennchen et al.* [2010] obtained nightside exospheric hydrogen densities that are about a factor of 1.5 - 5 times higher than densities in Table 1. However, they indicate evidence of an exospheric tail on the nightside. There are several possible explanations for the differences between these nightside observations and the dayside observations presented here. Two possibilities are solar cycle differences and erosion of the exosphere by charge exchange with the shocked solar wind at $R > 10\ R_E$. Measurements during a different part of the solar cycle and for a range of solar wind conditions and subsolar magnetopause locations are needed to determine why the dayside exospheric densities are lower than those on the nightside.

[19] **Acknowledgments.** Solar wind data are from the Wind spacecraft and provided through NSSDC CDAWeb. Support for this study comes from NASA's Explorer program. IBEX is the result of efforts from a large number of scientists, engineers, and others. All who contributed to this mission share in its success.

References

Anderson, B. J., S. A. Fuselier, S. P. Gary, and R. E. Denton (1994), Magnetic spectral signatures in the Earth's magnetosheath and plasma depletion layer, *J. Geophys. Res.*, *99*, 5877, doi:10.1029/93JA02827.

Collier, M. R., et al. (2001), Observations of neutral atoms from the solar wind, *J. Geophys. Res.*, *106*, 24,893, doi:10.1029/2000JA000382.

Collier, M. R., T. E. Moore, M.-C. Fok, B. Pilkerton, S. Boardsen, and H. Khan (2005), Low-energy neutral atom signatures of magnetopause motion in response to southward B_z, *J. Geophys. Res.*, *110*, A02102, doi:10.1029/2004JA010626.

Funsten, H. O., et al. (2009), The Interstellar Boundary Explorer High Energy (IBEX-Hi) Neutral Atom Imager, *Space Sci. Rev.*, *146*, 75, doi:10.1007/s11214-009-9495-8.

Fuselier, S. A., E. G. Shelley, and D. M. Klumpar (1988), AMPTE/CCE observations of shell-like He^{2+} and O^{6+} distributions in the Earth's magnetosheath, *Geophys. Res. Lett.*, *15*, 1333, doi:10.1029/GL015i012p01333.

Fuselier, S. A., et al. (2009), The IBEX-Lo Sensor, *Space Sci. Rev.*, *146*, 117, doi:10.1007/s11214-009-9495-8.

Gosling, J. T., and A. E. Robson (1985), Ion reflection, gyration, and dissipation at supercritical shocks, in *Collisionless Shocks in the Heliosphere: Reviews of Current Research*, *Geophys. Monogr.*, vol. 35, edited by B. T. Tsurutani, and R. G. Stone, pp. 141–152, AGU, Washington D. C.

Gosling, J. T., M. F. Thomsen, S. J. Bame, and C. T. Russell (1989), Ion reflection and downstream thermalization at the quasi-parallel bow shock, *J. Geophys. Res.*, *94*, 10,027, doi:10.1029/JA094iA08p10027.

Hosokawa, K., S. Taguchi, S. Suzuki, M. R. Collier, T. E. Moore, and M. F. Thomsen (2008), Estimation of magnetopause motion from low-energy neutral atom emission, *J. Geophys. Res.*, *113*, A10205, doi:10.1029/2008JA013124.

Lindsay, B. G., and R. F. Stebbings (2005), Charge transfer cross sections for energetic neutral atom data analysis, *J. Geophys. Res.*, *110*, A12213, doi:10.1029/2005JA011298.

McComas, D. J., et al. (2009a), IBEX-Interstellar Boundary Explorer, *Space Sci. Rev.*, *146*, 11, doi:10.1007/s11214-009-9495-8.

McComas, D. J., et al. (2009b), First global observations of the interstellar interaction from the interstellar boundary exlporer, *Science*, *326*, 959, doi:10.1126/science.1180906.

McComas, D. J., et al. (2009c), Lunar backscatter and neutralization of the solar wind: First observations of neutral atoms from the moon, *Geophys. Res. Lett.*, *36*, L12104, doi:10.1029/2009GL038794.

Moore, T. E., et al. (2000), The low-energy neutral atom imager for IMAGE, *Space Sci. Rev.*, *91*, 155, doi:10.1023/A:1005211509003.

Ogilvie, K. W., et al. (1995), SWE, a comprehensive plasma instrument for the Wind spacecraft, *Space Sci. Rev.*, *71*, 55-77, doi:10.1007/BF00751326.

Østgaard, N., S. B. Mende, H. U. Frey, G. R. Gladstone, and H. Lauche (2003), Neutral hydrogen density profiles derived from geocoronal imaging, *J. Geophys. Res.*, *108*(A7), 1300, doi:10.1029/2002JA009749.

Petrinec, S. M., and C. T. Russell (1997), Hydrodynamic and MHD equations across the bow shock and along the surfaces of planetary obstacles, *Space Sci. Rev.*, *79*, 757–791, doi:10.1023/A:1004938724300.

Shue, J.-H., et al. (1998), Magnetopause location under extreme solar wind conditions, *J. Geophys. Res.*, *103*(A8), 17,691–17,700, doi:10.1029/98JA01103.

Taguchi, S., S.-H. Chen, M. R. Collier, T. E. Moore, M.-C. Fok, K. Hosokawa, and A. Nakao (2005), Monitoring the high-altitude cusp with low-energy neutral atom imager: Simultaneous observations from IMAGE and Polar, *J. Geophys. Res.*, *110*, A12204, doi:10.1029/2005JA011075.

Zoennchen, J. H. (2010), 3-D-Geocoronal hydrogen density derived from TWINS Ly-α-data, *Ann. Geophys.*, *28*, 1221, doi:10.5194/angeo-28-1221-2010.

H. O. Funsten, Los Alamos National Laboratory, Los Alamos, NM 87545, USA.

S. A. Fuselier, S. M. Petrinec, and K. J. Trattner, Lockheed Martin Advanced Technology Center, 3251 Hanover St., Palo Alto 94304, CA, USA. (stephen.a.fuselier@lmco.com)

D. Heirtzler, H. Kucharek, and E. Möbius, Institute for the Study of Earth, Oceans and Space, University of New Hampshire, Durham, NH 03824, USA.

P. Janzen and D. B. Reisenfeld, Department of Physics and Astronomy, University of Montana, 32 Campus Dr., Billings, MT 59812, USA.

D. J. McComas, Southwest Research Institute, P.O. Drawer 28510, San Antonio, TX 78228, USA.

T. E. Moore, Heliophysics Science Division, NASA Goddard Space Flight Center, 8800 Greenbelt Rd., Greenbelt, MD 20771, USA.

N. A. Schwadron, Astronomy Department, Boston University, 725 Commonwealth Ave., Boston, MA 02215, USA.

P. Wurz, Physics Institute, University of Bern, CH-3012 Bern, Switzerland.